ELSEVIER

Journal of Molecular Catalysis A: Chemical 141 (1999) 193–203

JOURNAL OF MOLECULAR CATALYSIS A: CHEMICAL

Synthesis of methylamines from CO_2, H_2 and NH_3 over Cu–Mg–Al mixed oxides

Steffen M. Auer, Silvia V. Gredig, René A. Köppel, Alfons Baiker *

Laboratory of Technical Chemistry, Swiss Federal Institute of Technology, ETH Zentrum, CH-8092 Zürich, Switzerland

Abstract

The synthesis of methylamines from carbon dioxide, hydrogen, and ammonia has been studied over catalysts derived from Cu–Mg–Al lamellar double hydroxides (LDH) with hydrotalcite-like structure. Catalysts containing 33 at.% Cu(II) related to the total metal content, with different ratios of Mg(II) to Al(III), and a binary Cu–Al catalyst containing 67 at.% Cu were prepared by precipitation of metal nitrates with sodium carbonate. The effect of sample composition and of calcination temperature on the catalytic behaviour has been investigated. Catalytic tests were performed in a fixed-bed microreactor in the temperature range 473–573 K and at 0.6 MPa total pressure. Activity for methylamine formation increased for the ternary catalysts with increasing ratio $x = M(III)/[M(II) + M(III)]$. Maximum activity was observed for a catalyst with $x = 0.33$, for which XRD analysis indicated a pure hydrotalcite-like phase. Increasing the calcination temperature of this sample from 673 K to 773 K improved the activity, whereas a significant loss in activity was observed when calcined at 873 K. This behaviour could be traced to the copper surface area, which increased from 4 to 14 $m^2\ g^{-1}$ (773 K) and then decreased to 9 $m^2\ g^{-1}$ (873 K), depending on calcination temperature. After catalytic testing the catalysts calcined up to 773 K consisted of dispersed copper in an amorphous oxide matrix, whereas calcination at 873 K caused the additional formation of $CuAl_2O_4$. Distribution of the methylamines was similar for all catalysts with the fraction of monomethylamine being higher than 80%, besides of smaller amounts of di- and trimethylamine. Other carbon containing products observed were carbon monoxide, formed by the reverse water–gas shift reaction (RWGSR), and methanol in the absence of ammonia in the feed. No general correlation between either BET or copper surface area and catalytic activity was observed. However, for the Cu–Mg–Al catalyst with $x = 0.33$ calcined at different temperatures activity for methylamine formation roughly parallelled the copper surface area measured by N_2O-titration.

Keywords: Methylamine synthesis; Carbon dioxide; Cu–Mg–Al mixed oxide; Layered double hydroxide; LDH; Hydrotalcite

1. Introduction

Conversion of CO_2 to valuable chemicals or fuels has been a major goal of catalytic research in recent years. In the presence of suitable catalysts, carbon dioxide can be efficiently reduced to methanol, methane, hydrocarbons, or formic acid and its derivatives [1–5]. Recently, we have demonstrated that methylamines (MA) can be produced from CO_2, H_2 and NH_3 over $Cu–Al_2O_3$ catalysts, affording monomethylamine as the main product [6,7].

Methylamines are produced commercially by the exothermic reaction of methanol with ammonia in the presence of solid acid catalysts

* Corresponding author. Tel.: +41-1-632-31-53; Fax: +41-1-632-11-63; E-mail: baiker@tech.chem.ethz.ch

1381-1169/99/$ - see front matter
PII: S1381-1169(98)00263-5

[8,9]. Thermodynamics of this reaction favour the formation of trimethylamine (TMA), whereas market demand is greater for monomethylamine (MMA) and especially dimethylamine (DMA). In industrial practice, selectivity to TMA is reduced either by application of shape-selective zeolites or by recycling of TMA combined with high NH_3 to methanol ratios [9].

In our studies on CO_2 hydrogenation, MMA was the favoured amine product [6,7]. It was proposed that acidic sites are involved in at least one of the reaction steps. However, strong acidity does not result in higher activity of the catalyst, probably due to strong adsorption of NH_3 and of product methylamines on acidic sites [10]. Based on NH_3-TPD experiments it was suggested that high activity in methylamine synthesis over supported copper catalysts is associated with appropriate acidic properties of the catalyst surface. Highest activity in methylamine synthesis was found for supports with an isoelectric point in the range 6–8 [10]. Hence, active catalysts should contain a medium acidity or basicity, in combination with a high dispersion of copper.

Lamellar double hydroxides (LDHs) are materials combining medium to high basicity and high dispersion of the constituents. They consist of positively charged metal hydroxide layers separated from each other by anions and water molecules. The layers contain metal ions of at least two different oxidation states. The most common case of di- and trivalent cations leads to the general chemical formula $[M(II)_{1-x}M(III)_x(OH)_2]^{x+}\ (A^{n-})_{x/n} \cdot mH_2O$, where x refers to the $M(III)/[M(II) + M(III)]$ ratio ranging between ca. 0.25 and 0.4 [11]. The positive charge of the metal hydroxide layers is compensated by interstitial layers built of anions A^{n-} and crystal water. In heterogeneous catalysis, LDHs are often used after calcination and subsequent reduction of the active component, thus forming highly dispersed metal/metal oxide systems [12–14]. As regards methylamine formation from CO_2, H_2 and NH_3, calcined and reduced LDHs containing highly dispersed copper combined with a matrix of medium basicity are expected to fulfill the requirements for an active catalyst.

The aim of this study was to elucidate the relation between structural and chemical properties of different Cu–Mg–Al LDHs and mixed oxides and their catalytic behaviour in the synthesis of MAs from CO_2, H_2 and NH_3.

2. Experimental

2.1. Catalyst preparation

Various amounts of $Cu(NO_3)_2 \cdot 3H_2O$, $Mg(NO_3)_2 \cdot 6H_2O$ and $Al(NO_3)_3 \cdot 9H_2O$ (total metal nitrates = 0.24 mol) were dissolved in 500 ml distilled water and transferred into a 1-l five-necked flask equipped with propeller mixer, reflux condenser, pH-meter (Metrohm 614), thermocouple and feeding unit for liquids (Metrohm 665 Dosimat). This system was equilibrated at 333 ± 2 K under vigorous stirring. Subsequently, 300 to 500 ml 0.75 M Na_2CO_3 solution were slowly added to the metal nitrate solution over a period of 2 h until a pH of 8 was reached. The light-blue suspension was stirred for 15 h at room temperature and filtered. The precipitates were thoroughly washed with distilled water and dried for 24 h at 363 K and a pressure < 10 kPa. The obtained samples were calcined for 4 h under reduced pressure (15 Pa) at different temperatures.

2.2. Catalyst characterization

Catalysts were investigated with regard to their structural and chemical properties by means of thermoanalytical measurements (TG/DTA) combined with mass spectrometry (MS), X-ray powder diffraction (XRD), temperature programmed reduction (TPR), N_2O titration and N_2 physisorption.

XRD patterns were measured on a Siemens D5000 powder X-ray diffractometer. Diffractograms were recorded with detector-sided Ni-

filtered Cu K_α radiation (40 mA, 40 kV) over a 2θ-range of 2° to 70° and a position sensitive detector using a step size of 0.01° and a step time of 2.5 s. Mean crystallite sizes of copper ($\bar{d}_{Cu}$) were estimated from the half-width of the (111) reflection of Cu using the Scherrer equation [15,16] and taking into account the contribution of instrumental line broadening of $2\theta = 0.08°$ [17].

Thermogravimetric (TG) and differential thermoanalytical (DTA) studies in the temperature range 298 K to 1323 K were carried out on a Netzsch STA 409. Measurements were performed in flowing Ar using α-Al_2O_3 as a reference and a heating rate of 10 K min^{-1}. Evolving gases were monitored on-line using a Balzers QMG 420 quadrupole mass spectrometer connected to the thermoanalyzer by a heated capillary.

The apparatus used for the TPR studies has been described previously [18]. TPR profiles were measured under the following conditions: sample weight 60 mg, heating rate 10 K min^{-1}, flow rate 75 ml min^{-1} of 5% H_2 in Ar.

Cu surface areas were determined by N_2O-titration using a pulse technique similar to that reported by Evans et al. [19,20]. Samples were reduced in flowing H_2/Ar (5% H_2, 75 cm^3 min^{-1}) by heating from 373 K to 548 K at 5 K min^{-1}. Subsequently the samples were held at this temperature for 15 min and then exposed to a flux of 75 cm^3 min^{-1} pure hydrogen for 30 min at 548 K. The hydrogen was purged with 50 cm^3 min^{-1} He at 548 K. After cooling to 363 K under He, pulses of nitrous oxide (0.5 cm^3) were injected. Copper metal surface areas were calculated assuming $1.46 \cdot 10^{19}$ copper atoms per m^2 [19] and an adsorption stoichiometry of $Cu_S/O_{ads} = 2$. The accuracy of the copper surface area measurements was within 5%.

BET surface areas (S_{BET}), mean cylindrical pore diameters ($\langle d_p \rangle$) and specific adsorption pore volumes (V_p) were determined by nitrogen physisorption at 77 K using a Micromeritics ASAP 2000 instrument. Prior to measurement, the samples were degassed to 0.1 Pa at 473 K. S_{BET} was determined in a relative pressure range between $0.05 < p/p_0 < 0.2$ assuming a cross-sectional area of 0.162 nm^2 for the nitrogen molecule. Pore size distributions were calculated applying the Barrett–Joyner–Halenda (BJH) method [21] to the desorption branch of the isotherms [22]. The assessments of microporosity were made from *t*-plot constructions ($0.3 < t < 0.5$ nm) using the Harkins–Jura correlation [23].

2.3. Catalytic tests

Catalytic tests were performed using a stainless steel continuous tubular fixed-bed microreactor (length: 35 cm, diameter: 0.8 cm) at a total pressure of 0.6 MPa in the temperature range 473 K to 573 K. The experiments were carried out using 3 g catalyst and a reactant flow rate of 150 cm^3 min^{-1} (GHSV = 2250 h^{-1}). The feed gas, containing 60 mol% H_2, 20 mol% CO_2, 0–20 mol% NH_3 and N_2 as a balance, was mixed from cylinder gases using mass flow controllers. The reaction gases employed in the experiments were CO_2 (99.995%), H_2 (99.999%), NH_3 (99.3%) and N_2 (99.995%). The product gas mixture was analysed using a Hewlett-Packard 5890A gas chromatograph equipped with two thermal conductivity detectors and with a SPB-1 fused silica capillary column (60 m, 0.53 mm I.D., 5 μm film) and a Porapak QS column (5 m, 1/8 in. O.D., 80–100 mesh), arranged in parallel.

Before catalytic tests the catalysts were reduced at 473 K in a hydrogen/nitrogen mixture by increasing the mole fraction of hydrogen stepwise (30 min per step) in the sequence 10/20/50 to 100%. After increasing the temperature to 513 K for 30 min, hydrogen was replaced by the reaction gas mixture.

3. Results

Three ternary Cu–Mg–Al mixed oxides of type $[Cu_{0.33}Mg_{(0.67-x)}Al_x - CO_3]$ [24], which

contained 33 at.% of Cu(II) related to the total metal content, have been prepared. The *x*-value of the samples, i.e., the ratio of Al(III) to total metal content, was varied between 0.25 and 0.33. The composition of the ternary catalysts is fully defined by the *x*-value. We will therefore use the denotation $[Cu–x]_T$ for the ternary samples [25], where *T* [K] represents the calcination temperature. Uncalcined catalysts are indicated by the subscripts uc. In addition to the ternary samples, one binary Cu–Al mixed oxide of type $[Cu_{0.67}Al_{0.33}–CO_3]$ has been prepared and is denoted $[Cu–Al]_T$ in the following.

3.1. Catalyst characterization

The effect of the preparation variables on the structural and catalytic properties is investigated considering catalyst composition and the influence of calcination as parameters. The effect of calcination is exemplarily shown for catalyst [Cu–0.33].

3.1.1. Influence of calcination temperature

Gases evolved during thermal decomposition of $[Cu–0.33]_{uc}$ in Ar were monitored by TG/MS (Fig. 1). Up to 773 K, the decomposition pattern is characteristic for all LDHs [26], showing the evolution of H_2O and CO_2 and a concomitant weight loss of ca. 30%. However, further increase in temperature leads to a second evolution of CO_2 at 870 K, typical for Cu–Mg–Al LDHs [25].

Crystalline phases of [Cu–0.33] after calcination at different temperatures, determined by XRD, are depicted in Fig. 2a. The uncalcined sample $[Cu–0.33]_{uc}$ showed the characteristic diffraction pattern of hydrotalcite-like phases (JCPDS 37-0630) [27]. Upon calcination crystallinity of this phase declined, leading to a predominantly amorphous catalyst after calcination at 673 K and 773 K, respectively. With higher calcination temperatures (873 K), crystalline CuO (JCPDS 41-0254), MgO (JCPDS 4-0829) and $CuAl_2O_4$ (JCPDS 33-0448) phases were formed [27].

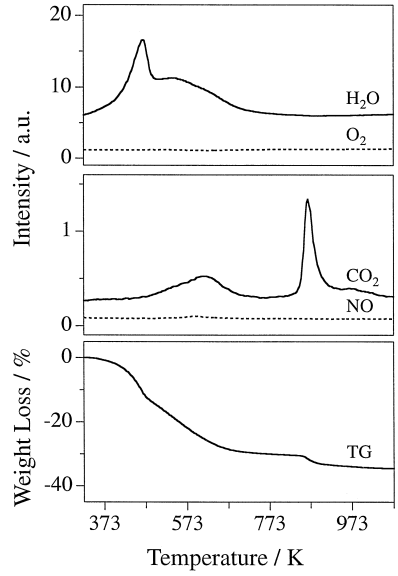

Fig. 1. Thermoanalytical investigation of [Cu–0.33] in Ar. Top: Evolving gases during thermal decomposition monitored by MS, ion intensities of $m/z = 18$ (H_2O) and $m/z = 44$ (CO_2); bottom: corresponding TG curve. Heating rate: 10 K min^{-1}.

The diffraction patterns after reduction and amination reaction shown in Fig. 2b are dominated by reflections of Cu (JCPDS 4-0836) [27]. For $[Cu–0.33]_{673}$ and $[Cu–0.33]_{773}$, calcined below the second CO_2 evolution at 870 K, a lower degree of crystallinity of the Cu phase was observed than with $[Cu–0.33]_{uc}$ and $[Cu–0.33]_{873}$ (Fig. 2b), as also indicated by the corresponding copper crystallite sizes listed in Table 1. Apart from the Cu phase, Cu_2O (JCPDS 5-0667), formed by the oxidation of Cu upon exposure of the catalyst to air, was detected for the catalysts after catalytic testing. In the case of $[Cu–0.33]_{873}$ traces of $CuAl_2O_4$ (JCPDS 33-0448) were additionally observed in the XRD pattern.

The reduction behaviour of [Cu–0.33] calcined at different temperatures is shown in Fig. 3. Two temperature regions of maximum hydrogen consumption rate at ca. 523 K and around 610 K were observed in the TPR-profiles, indicating different reducibility of the Cu(II) species. The TPR profiles of $[Cu–0.33]_{773}$ and $[Cu–0.33]_{873}$ only exhibited the maximum at lower

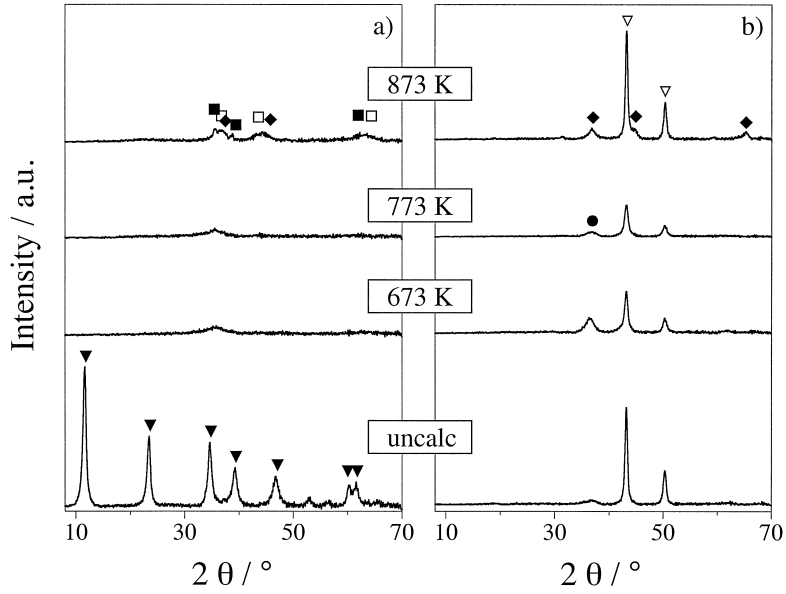

Fig. 2. XRD analysis of [Cu–0.33] calcined at different temperatures, (a) before and (b) after catalytic reaction. (▼) Hydrotalcite (HT) phase, (■) CuO, (□) MgO, (♦) $CuAl_2O_4$, (▽) Cu, (●) Cu_2O.

temperature, whereas $[Cu–0.33]_{673}$ showed a dominant peak at 620 K and a smaller feature at 523 K. Besides of a distinct maximum at 603 K, the TPR profile of $[Cu–0.33]_{uc}$ is characterized by a small peak at 500 K, which is attributed to the reduction of nitrate residues in the catalyst.

The textural properties of the catalysts are summarized in Table 1. All adsorption/desorption isotherms were of type-IV with a type-H3 hysteresis according to IUPAC [28], which is generally observed for mesoporous aggregates of plate-like particles. Microporosity of all samples, before and after reaction, was negligible. Pore volumes (V_p) and mean pore diameters ($\bar{d}_p$) of [Cu–0.33] were equivalent within experimental error for all calcination temperatures.

Table 1
Morphological properties of Cu–Mg–Al catalysts with different composition and calcined at different temperature, determined by N_2 physisorption and XRD

Catalyst[a]	Before reaction			After reduction/reaction				
	S_{BET} (S_t)[b] [$m^2\ g^{-1}$]	V_p (N_2)[c] [$cm^3\ g^{-1}$]	$\langle d_p \rangle$[d] [nm]	S_{BET} (S_t)[b] [$m^2\ g^{-1}$]	V_p (N_2)[c] [$cm^3\ g^{-1}$]	$\langle d_p \rangle$[d] [nm]	$\bar{d}_{Cu}$ (XRD)[e] [nm]	S_{Cu} (N_2O)[f] [$m^2\ g^{-1}$]
$[Cu–Al]_{673}$	30 (3)	0.19	22	27 (0)	0.19	24	40	5
$[Cu—0.33]_{673}$	65 (3)	0.49	22	87 (3)	0.49	16	16	7
$[Cu—0.29]_{673}$	95 (0)	0.65	22	108 (3)	0.67	20	20	10
$[Cu—0.25]_{673}$	90 (7)	0.68	28	93 (7)	0.60	22	35	5
$[Cu—0.33]_{uc}$	65 (0)	0.47	25	150 (0)	0.64	15	20	4
$[Cu—0.33]_{773}$	65 (3)	0.51	24	94 (0)	0.50	17	14	14
$[Cu—0.33]_{873}$	95 (0)	0.49	20	112 (0)	0.62	18	23	9

[a] Denotation of catalysts are explained at the beginning of Section 3.
[b] BET surface area (specific micropore surface area derived from *t*-plot analysis).
[c] BJH cumulative desorption pore volume.
[d] Mean pore diameter, $\langle d_p \rangle = 4\ V_p\ (N_2)/S_{BET}$.
[e] Copper crystallite size of samples after catalytic reaction determined from XRD line broadening.
[f] Copper surface area of samples after calcination measured by N_2O-titration.

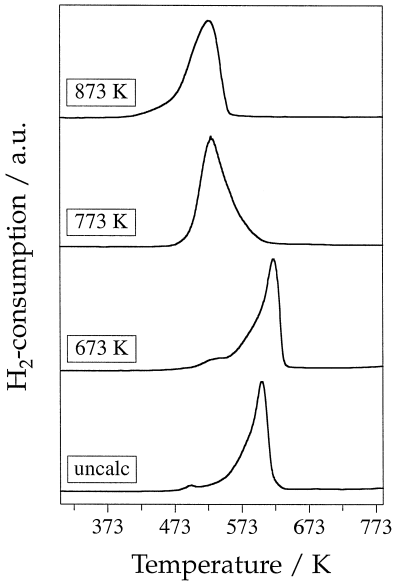

Fig. 3. Temperature programmed reduction profiles of [Cu–0.33], calcined at different temperatures under reduced pressure (15 Pa) for 4 h. TPR in 5% H_2/Ar, heating rate 10 K min^{-1}.

However, the BET surface area of $[Cu–0.33]_{873}$ was significantly higher than the surface areas of the catalysts calcined at lower temperatures. After reduction and catalytic reaction, S_{BET} of [Cu–0.33] was markedly higher for all calcination temperatures, with the effect being most pronounced for the uncalcined sample. In addition, the mean pore diameters slightly decreased.

The copper surface areas (S_{Cu}) of samples calcined at different temperature were determined by N_2O-titration (Table 1). Calcination at temperatures up to 773 K resulted in an increase of S_{Cu} from 4 to 14 m^2 g^{-1}, which then decreased to 9 m^2 g^{-1} for a calcination temperature of 873 K. A similar trend is observed for the mean copper crystallite sizes ($\bar{d}_{Cu}$) estimated from the XRD-line broadening of the samples after catalytic testing, which showed smallest crystallites for the catalyst calcined at 773 K (Table 1).

3.1.2. Influence of composition

Catalysts with different composition are compared after calcination at 673 K. At this temperature the samples have evolved the main fraction of H_2O, but not the second part of CO_2 (Fig. 1).

Crystalline phases of the differently composed samples after drying, calcination and catalytic reaction, respectively, were determined by XRD analysis (Fig. 4). After drying (Fig. 4a), three crystalline phases were detected, a hydrotalcite-like phase (HT-phase; JCPDS 37-0630), a magnesium–copper hydroxide nitrate phase

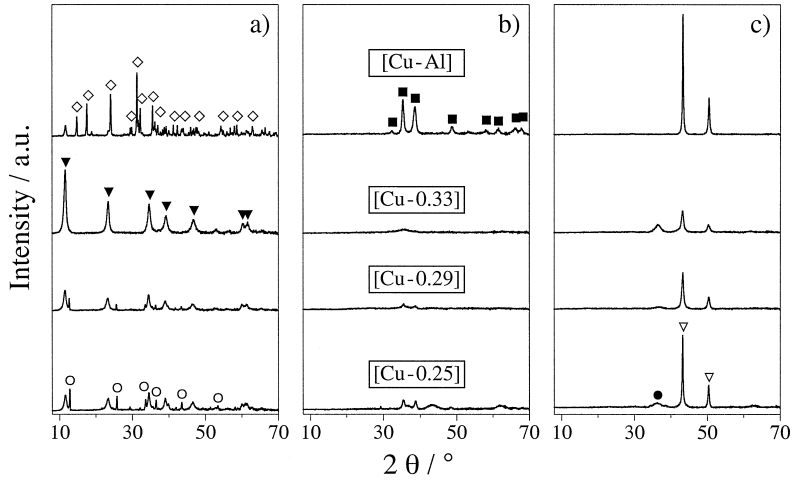

Fig. 4. X-ray diffraction patterns of [Cu–0.25], [Cu–0.29], [Cu–0.33] and [Cu–Al], (a) uncalcined (raw), (b) calcined at 673 K and (c) after catalytic reaction. (▼) Hydrotalcite (HT) phase, (○) Cu–Mg hydroxide nitrate (MgCu-phase), (■) CuO, (◇) Malachite, (▽) Cu, (●) Cu_2O.

(MgCu-phase; JCPDS 26-1221, 15-0014) and a malachite phase (JCPDS 41-1390) [27]. With increasing *x*-value of the ternary catalysts, the fraction of the crystalline HT-phase increased, whereas the fraction of the crystalline MgCu-phase decreased. In $[Cu–0.25]_{uc}$ and $[Cu–0.29]_{uc}$ both phases coexisted, whereas $[Cu–0.33]_{uc}$ showed only reflections due to the HT-phase. The XRD pattern of the binary catalyst $[Cu–Al]_{uc}$ exhibited reflections characteristic of malachite and only weak reflections of the HT-phase. After calcination at 673 K, all samples contained CuO (JCPDS 41-0254) [27] with different degrees of crystallinity (Fig. 4b). CuO of high crystallinity was found for the binary catalyst $[Cu–Al]_{673}$, whereas crystallinity was low for the ternary catalysts. For the latter, crystallinity moreover decreased with increasing *x*-value. Fig. 4c depicts diffraction patterns after reduction and catalytic testing. The XRD patterns are dominated by reflections due to Cu (JCPDS 4-0836) [27]. The higher the crystallinity of CuO before reduction/reaction, the higher was the crystallinity of Cu after reaction (compare $\bar{d}_{Cu}$ listed in Table 1). Apart from the Cu phase, Cu_2O (JCPDS 5-0667) was detected in the ternary samples due to oxidation of Cu upon exposure of the catalysts to air.

BET surface areas (S_{BET}) and pore volumes (V_p) were higher for the ternary catalysts than for the binary $[Cu–Al]_{673}$ (Table 1). For the ternary samples S_{BET} and V_p were significantly lower for $[Cu–0.33]_{673}$ compared to the samples with lower *x*-value. Mean pore diameters of all samples were in the same order of magnitude. During reduction and catalytic reaction, S_{BET} of the ternary samples increased and mean pore diameters slightly decreased, whereas the morphological data of the binary catalyst $[Cu–Al]_{673}$ were hardly altered.

Cu surface areas (S_{Cu}) of samples calcined at 673 K are listed in Table 1 together with mean copper crystallite sizes ($\bar{d}_{Cu}$). The ternary catalyst $[Cu–0.29]_{673}$ exhibited the highest Cu surface area of all samples, whereas S_{Cu} was lowest for $[Cu–Al]_{673}$ and $[Cu–0.25]_{673}$.

3.2. Catalytic behaviour

The only carbon-containing products detected during steady state catalytic measurements were mono-, di- and trimethylamine (MMA, DMA, TMA, respectively), carbon monoxide, and, in the absence of ammonia in the feed, methanol. Formation of HCN, as found in traces with supported copper catalysts [10], was not observed. No indication for catalyst deactivation was observed throughout the catalytic tests. Variation of the space velocity in the range 1500–3000 h^{-1} had only little influence on the catalytic behaviour.

The temperature dependence of the product distribution measured for $[Cu–0.33]_{773}$ is depicted in Fig. 5 (top). MMA is the favoured methylamine product over the whole temperature range investigated. Only small amounts of

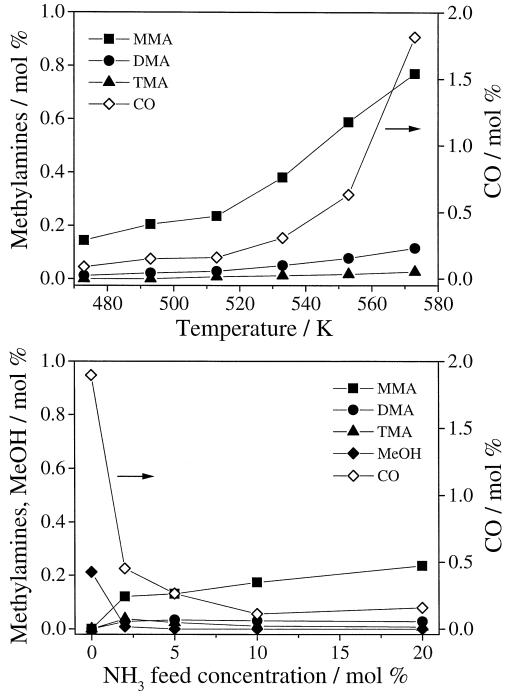

Fig. 5. Top: Temperature dependence of formation of methylamines and CO from CO_2, H_2 and NH_3 for catalyst [Cu–0.33] calcined at 773 K. Conditions: 3 g catalyst, 0.6 MPa, 150 cm^3 min^{-1} CO_2:NH_3:H_2 = 1:1:3. Bottom: Influence of NH_3 feed concentration on formation of products from CO_2, H_2 and NH_3 for catalyst [Cu–0.33] calcined at 773 K. Conditions: 3 g catalyst, 513 K, 0.6 MPa, 150 cm^3 min^{-1} CO_2:NH_3:H_2 = 1:0–1:3.

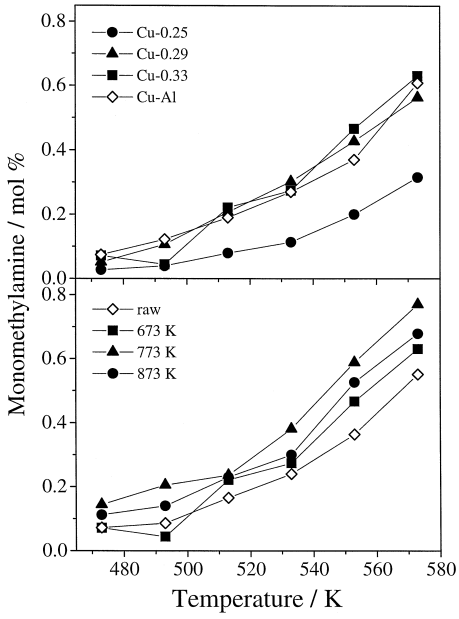

Fig. 6. Influence of catalyst composition for samples calcined at 673 K (top) and of calcination temperature for catalyst [Cu–0.33] (bottom), on monomethylamine formation from CO_2, H_2 and NH_3. Conditions: 3 g catalyst, 0.6 MPa, 150 cm^3 min^{-1} CO_2:NH_3:H_2 = 1:1:3.

DMA and TMA were detected, reaching a maximum concentration of 0.115 and 0.026 mol%, respectively, at 573 K. Formation of CO via the reverse water–gas shift reaction (RWGSR) increased above 513 K and developed to the main reaction for temperatures exceeding 543 K.

Without ammonia in the feed, methanol (0.21 mol%), carbon monoxide (1.9 mol%) and water were observed at 513 K for catalyst $[Cu–0.33]_{773}$ (Fig. 5, bottom). Upon addition of NH_3 to the feed, methanol formation was completely suppressed and CO formation markedly decreased to 0.16 mol% for a NH_3 concentration of 20 mol% in the feed. With increasing ammonia concentration, the amount of MMA increased, whereas formation of DMA and TMA showed a maximum at ammonia concentrations of 5 mol% (0.034 mol%) and at 2 mol% (0.038 mol%), respectively.

Similar overall dependencies of product formation on temperature and ammonia feed concentration were observed for the other catalysts investigated. However, NH_3 conversion and product distribution were greatly influenced by the sample composition and calcination temperature. The temperature dependence of MMA formation over the different catalysts calcined at 673 K is illustrated in Fig. 6 (top). MMA as the predominant methylamine product was produced in comparable amounts for $[Cu–0.29]_{673}$, $[Cu–0.33]_{673}$ and $[Cu–Al]_{673}$, whereas significantly less MMA was obtained with $[Cu–0.25]_{673}$. The influence of calcination temperature on MMA formation of catalyst [Cu–0.33] is presented in Fig. 6 (bottom). Independent of the reaction temperature, largest amounts of MMA were observed for the catalyst calcined at 773 K, whereas least MMA was produced with the uncalcined sample.

Table 2 summarizes the catalytic properties of the various catalysts in the synthesis of meth-

Table 2
Catalytic properties of different Cu–Mg–Al catalysts calcined at different temperatures

Catalyst[a]	Amine production rate [mol kg_{cat}^{-1} h^{-1}]	Methylamine distribution			Selectivity	
		MMA [%]	DMA [%]	TMA [%]	Methylamines [%]	CO [%]
$[Cu–Al]_{673}$	0.57	79	15	6	84	16
$[Cu—0.33]_{673}$	0.67	85	12	3	50	50
$[Cu—0.29]_{673}$	0.60	87	11	2	59	41
$[Cu—0.25]_{673}$	0.24	100	0	0	80	20
$[Cu—0.33]_{uc}$	0.52	86	11	3	71	29
$[Cu—0.33]_{773}$	0.83	86	11	3	52	48
$[Cu—0.33]_{873}$	0.75	86	12	2	55	45

Reaction conditions: 3 g catalyst, 553 K, 0.6 MPa, 150 cm^3 min^{-1} CO_2:NH_3:H_2 = 1:1:3.
[a] Denotation of catalysts are explained at the beginning of Section 3.

ylamines from $H_2/CO_2/NH_3$ mixtures under standard conditions at 553 K. For the ternary catalysts the catalytic activity, expressed as the amount of methylamines produced per hour and per kg catalyst, decreased with decreasing *x*-value. With regard to the distribution of the three methylamines a similar picture emerges for all catalysts, except $[Cu–0.25]_{673}$, which exclusively produced MMA up to 553 K. Selectivity to CO was lowest for the binary sample $[Cu–Al]_{673}$ and for $[Cu–0.25]_{673}$ (Table 2), which both contained well crystalline copper with relatively large crystallites after catalytic testing (Table 1).

4. Discussion

Depending on the sample composition and calcination temperature, a distinctly different behaviour of the catalysts in the synthesis of methylamines from $H_2/CO_2/NH_3$ is observed. The activity of the catalysts in relation to the bulk composition of the samples is presented in Fig. 7. For the ternary samples with constant Cu content, calcined at 673 K, conversion to methylamines increases with increasing *x*-value to reach a maximum for [Cu–0.33]. XRD revealed the presence of a pure hydrotalcite-like phase for this catalyst, whereas catalysts with lower *x*-value contained increasing amounts of a magnesium–copper hydroxide nitrate phase besides of the hydrotalcite-like phase. Note that the activity of the binary catalyst with double copper loading and $x = 0.33$ is slightly lower than observed for $[Cu–0.33]_{673}$, indicating that the copper loading has only a weak influence on the catalytic performance.

Increasing the calcination temperature from 673 K to 773 K resulted in higher methylamine formation activity for [Cu–0.33], whereas it declined at higher calcination temperature (873 K). After calcination at 673 or 773 K the catalysts were predominantly X-ray amorphous, whereas X-ray analysis revealed formation of crystalline $CuAl_2O_4$ for higher calcination temperature. For the catalysts calcined up to 773 K the second loss of CO_2, as evidenced by the thermoanalytical experiments, has not occurred thus indicating that a hydrotalcite-type phase is still present in these samples, as decomposition of copper or magnesium carbonates typically takes place at lower temperatures. After reduction and catalytic reaction the catalysts calcined at 673 and 773 K contained highly dispersed copper in an amorphous oxide matrix.

As evident from Table 1, no general correlation between either BET surface area or pore

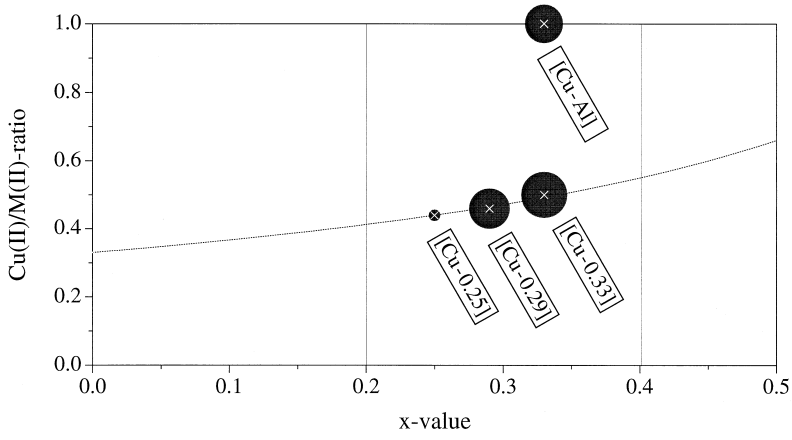

Fig. 7. Influence of catalyst composition on conversion to methylamines. The bulk composition of the Cu–Mg–Al catalysts calcined at 673 K is expressed as both [Cu(II)]/[M(II)] ratio and *x*-value ($x = [M(III)]/[M(II) + M(III)]$). Conversion to methylamines is proportional to the bubble diameter. Conditions: 553 K, 3 g catalyst, 0.6 MPa, 150 cm^3 min^{-1}, $H_2:CO_2:NH_3 = 3:1:1$.

structure and the catalytic activity is observed. The binary catalyst $[Cu–Al]_{673}$ with comparably low S_{BET} and V_p (N_2) showed similar high activity as found for $[Cu–0.33]_{uc}$ with highest BET surface area. Moreover, no general trend between the copper surface area measured by N_2O-titration and the catalytic activity is observed when considering all catalysts. However, for catalyst [Cu–0.33] calcined at different temperatures activity for methylamine formation correlates with the copper surface area. A similar observation has been reported for methanol synthesis from CO_2/H_2 feeds on copper catalysts [20], where a correlation between catalytic activity and copper surface area was only found within groups of similarly prepared catalysts.

In case of methylamine synthesis, copper surface area is not expected to be the only decisive parameter influencing the catalytic behaviour. Catalytic studies on various copper/metal oxide catalysts revealed that the surface acidity/basicity of the metal oxide component has some influence on the catalytic performance [10]. For the formation of methylamines from CO_2, H_2 and NH_3 on copper–alumina catalysts a mechanism has been proposed on the basis of findings in the amination of alcohols with ammonia, and of methanol synthesis from CO_2 and H_2. It was suggested that methylamine formation occurs mainly by the reaction of adsorbed ammonia with an aldehyde-type surface intermediate formed from CO_2 and H_2 and not via methanol [7,29]. The reaction sequence requires catalytic functions relevant in methanol synthesis as well as in the amination of alcohols, including the activation of ammonia. Activation of NH_3 as well as desorption of the product methylamines require appropriate acidity/basicity properties of the catalyst surface.

5. Conclusions

The influence of sample composition and of calcination temperature on the catalytic behaviour of catalysts derived from Cu–Mg–Al lamellar double hydroxides (LDH) with hydrotalcite-like structure has been investigated. Highest activity for the synthesis of methylamines from CO_2, H_2 and NH_3 has been obtained for a catalyst derived from a pure hydrotalcite-like precursor, whereas contribution of other precursor phases resulted in lower activity.

With increasing calcination temperature formation of methylamines increased, reaching a maximum for catalysts calcined at 773 K, and then decreased. Calcination at 673 or 773 K resulted in X-ray amorphous materials which upon reduction/catalytic testing transformed to highly dispersed copper in an amorphous oxide matrix. At higher calcination temperature formation of a $CuAl_2O_4$ phase was observed besides of microcrystalline copper oxide.

Distribution of the methylamines was similar for all catalysts with the fraction of monomethylamine being higher than 80%. Carbon monoxide, formed via the reverse water–gas shift reaction, was observed as a by-product. Methanol was only formed in the absence of ammonia in the feed.

Acknowledgements

Financial support by the Swiss National Fonds (Project No. 21-41850.94) and by the Bundesamt für Energiewirtschaft (Project-Nr. 21180) is gratefully acknowledged. S.M. Auer thanks the Fonds der Chemischen Industrie, Germany, for granting a stipendium.

References

[1] G.C. Chinchen, P.J. Denny, J.R. Jennings, M.S. Spencer, K.C. Waugh, Appl. Catal. 36 (1988) 1.
[2] M. Halmann, Chemical Fixation of Carbon Dioxide: Methods for Recycling CO_2 into Useful Products, CRC Press, Boca Raton, 1993.
[3] A. Baiker, R.A. Köppel, Proc. Int. Conf. on Carbon Dioxide Utilization, Bari, September 26–30, 1993, pp. 295–302.
[4] A. Baiker, R.A. Köppel, 3rd Int. Conf. on Carbon Dioxide Utilization, Norman, OK, 1995.
[5] P.G. Jessop, T. Ikariya, R. Noyori, Chem. Rev. 95 (1995) 259.

[6] S.V. Gredig, R.A. Koeppel, A. Baiker, J. Chem. Soc., Chem. Commun., (1995) 73.
[7] S.V. Gredig, R.A. Koeppel, A. Baiker, Catal. Today 29 (1996) 339.
[8] A. Baiker, J. Kijenski, Catal. Rev. Sci. Eng. 27 (1985) 653.
[9] A.B. Van Gysel, W. Musin, Ullmann's Encyclopädie der Technischen Chemie, Vol. 16, Verlag Chemie, Weinheim, 1974.
[10] S.V. Gredig, R. Maurer, R.A. Koeppel, A. Baiker, J. Mol. Catal. 127 (1997) 133.
[11] F. Cavani, F. Trifirò, A. Vaccari, Catal. Today 11 (1991) 173.
[12] S. Gusi, F. Pizzoli, F. Trifirò, A. Vaccari, G. Del Piero, Stud. Surf. Sci. Catal. 31 (1987) 753.
[13] E.C. Kruissink, L.E. Alzamora, S. Orr, E.B.M. Doesburg, L.L. Van Reijen, J.R.H. Ross, G. Van Veen, Stud. Surf. Sci. Catal. 3 (1979) 143.
[14] A. Bhattacharyya, US-Patent 5399537, 1995.
[15] P. Scherrer, Gött. Nachr. 2 (1918) 98.
[16] H.P. Klug, L.E. Alexander, X-Ray Diffraction Procedures for Polycrystalline and Amorphous Materials, Wiley, New York, 1974.
[17] N.C. Halder, C.N.J. Wagner, Acta Crystallogr. 20 (1966) 312.
[18] R.A. Koeppel, J. Nickl, A. Baiker, Catal. Today 20 (1994) 45.
[19] J.W. Evans, M.S. Wainwright, A.J. Bridgewater, D.J. Young, Appl. Catal. 7 (1983) 75.
[20] R.A. Koeppel, A. Baiker, A. Wokaun, Appl. Catal. A 84 (1992) 77.
[21] E.P. Barrett, L.G. Joyner, P.P. Halenda, J. Am. Chem. Soc. 73 (1951) 373.
[22] J.C.P. Broekhoff, Stud. Surf. Sci. Catal. 3 (1979) 663.
[23] W.D. Harkins, G. Jura, J. Chem. Phys. 11 (1943) 431.
[24] A. De Roy, C. Forano, K. El Malki, J.P. Besse, Anionic Clays: Trends in Pillaring Chemistry, Van Nostrand-Reinhold, New York, 1992.
[25] S.M. Auer, R. Wandeler, U. Göbel, A. Baiker, J. Catal. 169 (1997) 1.
[26] W.T. Reichle, S.Y. Kang, D.S. Everhardt, J. Catal. 101 (1986) 352.
[27] Mineral Powder Diffraction Data Files, JCPDS-International Center for Diffraction Data, Swarthmore, PA, 1991.
[28] K.S.W. Sing, D.H. Everett, R.A.W. Haul, L. Moscou, R.A. Pierotti, J. Rouquérol, T. Siemieniewska, Pure and Appl. Chem. 57 (1985) 603.
[29] S.V. Gredig, R.A. Koeppel, A. Baiker, Appl. Catal. 162 (1997) 249.